Research article

# Resin bound gold nanocomposites assisted SE/ATR-FTIR spectroscopy for detection of pymetrozine insecticide in vegetable samples

Anushree Saha [a,*], Ramsingh Kurrey [b], Manas Kanti Deb [b,**]

[a] Department of Chemistry, Kalinga University, Naya Raipur, Chhattisgarh, India
[b] School of Studies in Chemistry, Pt. Ravishankar Shukla University, Raipur, 492 010, Chhattisgarh, India

A B S T R A C T

The goal of this work was to assess the competence of organic hydrophobic resin bound gold nanocomposites (OH/R-AuNCs) for detection of pymetrozine insecticide from vegetable samples employing surface-enhanced/attenuated total reflectance-Fourier transform infrared (SE/ATR-FTIR) spectroscopy. The adsorption isotherm models, including the Langmuir, Freundlich and Temkin, are tested to reveal the interactive behaviour between the OH/R-AuNCs and pesticide. The adsorption occurs principally by London–Van der Waals dispersion interactions and hydrogen bonding interactions between the surface of OH/R-AuNCs materials and the hydrophobic part of pesticide molecule. The characteristic absorption band obtained at $3019.94$ $cm^{-1}$ was utilized for the quantitative analysis of pymetrozine insecticide in vegetable samples. The method was found to be accurate and precise, with mean recovery values in the range of 94.5–110 %, correlation coefficient of 0.992 %, and detection limit of 2.65 µg $mL^{-1}$. The adsorption efficiency of the designed OH/R-AuNCs significantly influences the SE/ATR-FTIR response of the pymetrozine around 90 %. The optimized and validated method was applied to determine the residual concentrations of the pymetrozine that had been applied to vegetable samples.

## 1. Introduction

Pesticides are a significant group of chemical compounds of interest to the environment. The determination of pesticides receives growing attention because of their high toxicity and water solubility [1]. The insecticides, herbicides and fungicides are different pesticide groups used to control the growth of unwanted vegetations, insects and fungus; mainly, they are used against plant pests and diseases [1,2]. The chemical industries have discovered and developed new replacement chemicals/pesticides for proficient crop production and avoided interruption of ideal cultivation prototypes [3,4]. Nowadays, registration and utilization are being done of different types of nitrogenous pesticides, like pymetrozine, sulfonylureas, imidacloprid, atrazine, metribuzine and other triazines, which are indicated as biological chemicals [3–5]. Among all the pesticides classes, pymetrozine is used as an insecticide (killing of insect) [5]. Pymetrozine [4, 5-dihydro-6methyl-4-(3-pyridinyl-methylene amino)-1, 2, 4-triazine-3 (2H)-one], is a pyridine azomethine compound (a triazine derivative). It is a novel and selective insecticide, effective as a prevailing antifeedant against aphids,

homopteran insects and plant hoppers, which annoys the nervous regulation of insects [6]. Due to the widespread use of pesticides, their residues are distinguished in the environment. The pymetrozine are providing us with undisputable benefits of a low-cost supply of high-quality vegetable samples such as fruits and vegetables. Since the fruit and vegetable crops are highly disposed to pest attacks, they are frequently sprayed in their existence series with insecticides like pymetrozine [7,8]. The United State Environmental Protection Agency (US-EPA) has classified pymetrozine as a potential human carcinogen [9–11]. The maximum level of pymetrozine in foodstuffs has been set to 138 nM ($3 \times 10^{-8}$ µg mL$^{-1}$) by the National Food Safety Standard [9,11]. It is, therefore, important to monitor pymetrozine insecticide in agricultural samples such vegetables and fruits are a major challenge.

Routine methods used in pesticide residue analysis are often time and solvent consuming due to sample preparation steps before the instrumental analysis. There are a number of methods such as colorimetry [6], gas chromatography (GC) [12], high-performance liquid chromatography (HPLC) [5], liquid chromatography with mass spectrometry (LC-MS) [13], differential pulse polarography (DPP) [14], electronic spectroscopy (ES) [15] have been reported for the detection/separation of insecticide like pymetrozine in different matrices. Most of the methods have been recommended on the basis of good sensitivity towards the detection of targeted analytes. However, all these analytical tools have major drawbacks, including complex instrumentation, lower selectivity, limited capacity, time-consumption, etc. The surface-enhanced Raman spectroscopy (SERS) is another powerful analytical tool that provides wonderful advantages, including low-cost and ultrasensitive characterization down to a single molecular level but for this application, the standard Raman scattering signal is too weak to be detectable. Surface-enhanced infrared spectroscopy (SEIRS) has been investigated as a potential tool to address these issues, and offers certain advantages such as reduced instrument size, fast measurement times, non-destructive sampling, and simple implementation [16,17]. The SERS method is simply sensitive to vibrational modes with changes in the polarizability of the molecules, whereas SEIRS offers an alteration of the dipolar moment during the vibration of the molecules [18]. The SEIRS technique, however, detects the molecules adsorbed on the surface of metal nanomaterials (MNMs) to produce physical and chemical ameliorations that increase the FTIR signal intensity [19,20]. At present, the SEIRS technique has been widely used in the removal of pollutants from water bodies [21,22]. Hence, a SEIRS method that is versatile enough to detect multiple pesticides on a food surface at trace levels that does not require the extraction or drying steps may offer certain advantages.

Novel substrates were created and used for the qualitative and quantitative analysis, even the surface assimilation and removal of pesticides from sample matrices. The surface phenomenon of any resin or polymeric adsorbent has a great affinity because of its low-cost, low energy consumption, simple operation and high affinity and efficiency. The Amberlite XAD-4 resin is a rigid, non-ionic, cross-linked macro-reticular copolymer of styrene and divinyl benzene matrix with high surface area and high molecular weight [23]. Polymeric adsorbent is used as solid support for the immobilization of metal nanoparticles such as R-AuNCs due to its physical properties of adsorption, chemical composition, surface area of resin nanocomposite and adsorbate structure improving the mechanism of determination of analyte [24–26]. The OH/R-AuNCs material is abundant, more chemically stable and reactive than simple Amberlite XAD-4 resin beads [27]. Therefore, OH/R-AuNCs coupled with SEIRS could be used as a comparatively reactive adsorbent substrate for the detection of pesticides at a very trace level on the basis of a physicochemical adsorption process. Although, we still see no report on the application of SEIRS on the pesticides of pymetrozine detected using modified OH/R-AuNCs as adsorbent in this work.

In this paper, we describe the SE/ATR-FTIR spectroscopic method for the detection of pymetrozine insecticide using OH/R-AuNCs in vegetable samples under the optimized conditions. The effect of pesticide chemical composition and structure as well as the nature of solid surfaces on the efficiency of adsorption was evaluated using adsorption isotherm models. The above research was mainly focused on the single IR spectrum of a whole sample with real-life applications tend to focusing on the distribution of insecticide on the surface of vegetable products. The advantages of the present method are its simplicity, selectivity, sensitivity, ease of fabrication, rapid detection, and excellent adsorption efficiencies for the quantification of pymetrozine in vegetable samples.
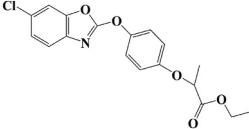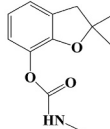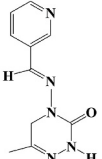
## 2. Experimental section

### 2.1. Apparatus

The Fourier transform infrared (FTIR) spectrometer (model: Nicolet iS10, ThermoFisher Scientific, Madison, USA) was used for the spectral measurements in the Mid-IR region at 4000-400 cm$^{-1}$. For the sample analysis, the attenuated total reflectance (ATR) accessories were used with a minimum resolution of 4 cm$^{-1}$. For spectral measurements, a ZnSe reflection crystal and a germanium coated potassium bromide (KBr) beam splitter was used with an approximately 15 scans for each spectrum of ATR-FTIR spectroscopy [20,21]. Other than these, Omnic 9 and TQ analysis software (Nicolat iS10) was used to acquire spectra.

The UV–Visible absorption bands were recorded for aqueous sample by using a Carry 60 UV–Visible spectrophotometer (Agilent Technology, Bombay) in the range of 200–800 nm along with a 1 cm quartz cuvette. Further, the electronic absorption spectra of solid materials were recorded in an EVOLUTION 220 integrated UV–Visible spectrophotometer (ThermoFisher Scientific, USA). The surface morphology and elemental composition were examined using a scanning electron microscope (SEM) with energy dispersive X-ray (SEM-EDX) analysis (model: JEOL JSM-6701F FE-SEM), respectively. The all aqueous solutions were prepared employing an ultrapure water system having resistivity and conductivity of 18.2 Ω and 0.055 µS/cm, respectively (ThermoFisher Scientific Barnstead Smart2pure, USA).

The preparation of nanocomposites and assimilation of solution mixtures were performed using a magnetic heating stirrer (5MLH, Mfd. Remi Equipment Pvt. Ltd, India) from 50 to 250 RPM. The pH measurement of the solution mixture was performed using a portable digital pH meter (model: 335, Systronics, India). Micropipettes were also used for the measurement of variable amounts of liquid volume (Glaxo smith Kline Pharmaceuticals; Vol. Range: 10–100 µL and 100–1000 µL). A Sartorius electronic balance with a precision of 10 mg (CP225D, AG Gottingen, Germany) was used for all weight measurements. To maintain the sensitivity of the method

**Table 1**
Employed pesticides physic-chemical properties and their uses.

| Name of Pesticides | Fenoxaprop-ethyl | Carbofuran | Pymetrozine |
|---|---|---|---|
| Molecular formula | $C_{18}H_{16}NO_5Cl$ | $C_{12}H_{15}NO_3$ | $C_{10}H_{11}N_5O$ |
| Molecular weight (g moL$^{-1}$) | 361.8 | 221.25 | 217.23 |
| Molecular Structure | | | |
| Class of pesticide | Herbicide | Insecticide | Insecticide |
| Type of pesticide | – | Carbamate | Triazines |
| Uses (control) | Unwanted vegetation | Insects and pests | Aphids and whiteflies |
| LD$_{50}$ | ~20 mgkg$^{-1}$ | ~8–14 mgkg$^{-1}$ | ~10–20 mgkg$^{-1}$ |

and to avoid any possible contamination during handling of all glassware, special care was taken.

### 2.2. Chemicals and solution preparation

The non-ionic Amberlite XAD-4 resin (Rohm and Hass, 1982), 40–60 mesh with high surface area and polymer matrix was purchased from Sigma-Aldrich, USA and used without further sanitization. Sodium chloride (NaCl), Mark (USA) was used for chlorinating the non-ionic resin beads. Chloroauric acid (HAuCl$_4$) and tri-sodium citrate (Na$_3$C$_6$H$_5$O$_7$) were purchased from Sigma-Aldrich (ACS reagent, ≥99.99 %, USA). The $2.5 \times 10^{-3}$ M precursor like HAuCl$_4$ and 1.0 % solution of Na$_3$C$_6$H$_5$O$_7$ were used for the preparation of functionalized AuNPs as nanomaterials. Potassium bromide, FT-IR grade, ≥99.99 % was purchased from Sigma-Aldrich (ACS reagent, ≥99.99 %, USA). All the pesticides (pymetrozine, carbofuran and fenoxaprop-ethyl) were purchased from Dr. Ehrenstofer GmbH, Germany.

The stock standard solutions of 1000 µg mL$^{-1}$ pesticides (pymetrozine, carbofuran and fenoxaprop-ethyl) were prepared by dissolving the appropriate amount of each pesticide in ultrapure water. The working standard solutions (10–100 µgmL$^{-1}$) were prepared by appropriate dilution of the stock standard solution of the above pesticides in ultrapure water. The physical and chemical properties of all pesticides and their uses are given in Table 1.

### 2.3. Sample collection and preparations

The vegetable samples (tomato, potato, brinjal and green bell pepper) were collected in clean polyethylene bags from the local vegetable markets of Raipur City, Chhattisgarh, India. Other than this, some vegetable samples were collected from agricultural crop zones because the massive amounts of pesticides were sprayed during the production of the samples by the farmers. Extraction started with 5.0 g of vegetable samples. After drying in the oven and grounding by mortar, 1.0 g of the powder was mixed with 1.0 mL of NaOH, sonicated for 3 min, and then left for 30 min at room temperature, in order to avoid degradation of some of the pesticides under alkaline conditions [16]. Afterward, the extracts were taken in a 50 mL volumetric flask for filtration with a 0.42 µm Whatman filter. The pH of all the sample's solution was adjusted to 4–5 because more soluble at a lower pH. Vegetable samples were kept in the dark at 4$^o$C from collection to analysis, being analyzed within different time intervals.

### 2.4. Developments of modified nanocomposites materials

Developments of modified nanocomposites materials for **detection** of pymetrozine insecticide in vegetable samples were completed by the following steps.

*Step A- Synthesis of citrate-capped AuNPs:* For the preparation of citrate capped AuNPs, 50 mL aqueous solution of HAuCl$_4$ as precursor ($2.5 \times 10^{-3}$ M) was taken in a 100 mL of conical flask and heated at 80 °C in over a magnetic heating stirrer for 30 min. A 0.6 mL of 1.0 % tri-sodium citrate (Na$_3$C$_6$H$_5$O$_7$) solution was added to the above solution with continuously stirring. After 50 s, the solution mixture was turned into faint blue color and then a dark red color indicating the formation of citrate-capped AuNPs (Fig. 1(a)). The citrate-capped AuNPs were used for the preparation of OH/R-AuNCs as nano-adsorbents.

*Step B- Preparation of OH/R-AuNCs:* The non-ionic Amberlite XAD-4 resin (2.0 g) was treated with 50 mL of 0.2 M NaCl solution to activate resin beads on the basis of ion-exchange process. After 1 h, the solution mixture was filtered and washed several times with ultrapure water to remove excess unreacted NaCl. The chlorinated resin beads were dried using desiccators to remove water moiety. The immobilized OH/R-AuNCs were prepared by loading 50 mL of $2.5 \times 10^{-3}$ M dispersed AuNPs onto the 1.0 g of chlorinated resin beads. The yellowish colour of the resin beads slowly changed into a blackish colour. After complete immobilization, OH/R-AuNCs were filtered and washed with water to remove unbound AuNPs. The formation of OH/R-AuNCs was confirmed by characterization through FTIR, SEM, XPS and UV–Visible spectrometer and used as a modified substrate for the detection of pesticide at very trace level. Fig. 1(b) shows the preparation of OH/R-AuNCs materials. The XRD image for the confirmation of formation of nanocomposite
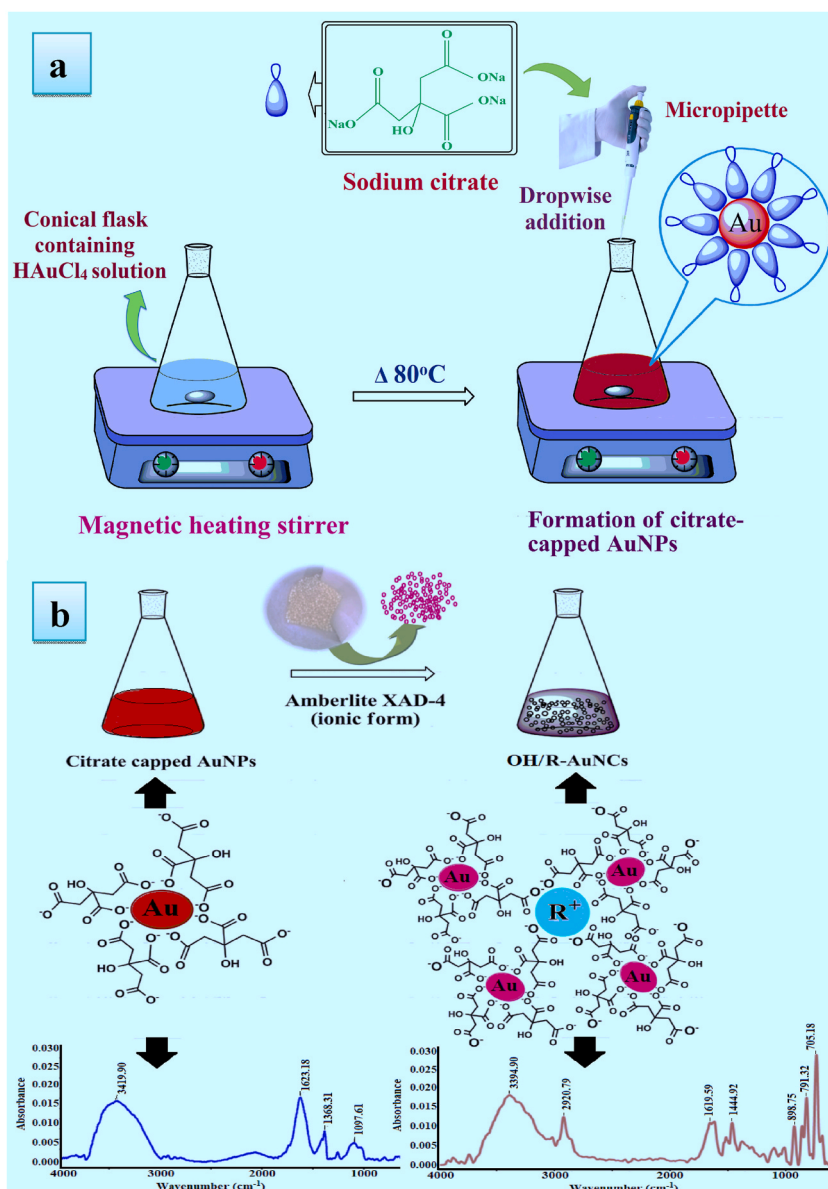
**Fig. 1.** Schematic diagram for preparation of citrate capped AuNPs (50 mL = $C_{2.5 \times 10^{-3} \, M}$ of AuNPs and 0.6 mL = $C_{1\%}$ of $Na_3C_6H_5O_7$) (a) and preparation of resin beads for OH/R-AuNCs as a chemical sensor along with functionalized AuNPs (b).

material is shown Figure S1 (a-b). The XRD pattern of free resin beads showed no peak due to the amorphous nature of polystyrene beads. A typical XRD pattern of R-AuNCs shows broad Bragg reflections, indicating that AuNPs are formed above the surface of polystyrene beads as a result of the immobilization process onto the resin beads.

### 2.5. Mass transfer model and SE/ATR-FTIR spectroscopic procedure

Fig. 2 depicts the schematic procedure for determination of pesticide using OH/R-AuNCs as modified substrate in SE/ATR-FTIR spectroscopy. The instrument (FTIR) was purged for 30 min with >99.99 % analytical grade liquid nitrogen using the iS10, iZ10 external purge kit, ThermoFisher Scientific, prior to analysis of samples for negligible atmospheric aberration, as water vapor and $CO_2$ in the sample chamber might lead to additional obscure peaks [22,28]. This method is based on an external mass transfer model for pesticide detection and IR signal amplification on the surface of an OH/R-AuNCs adsorbent. For this, firstly, 5.0 mL of pesticide solutions in different concentrations such as 10–100 μg mL$^{-1}$ were taken in 10 mL of conical flasks separately. Afterward, the pH of all the sample solutions was maintained at 4.0 by pouring in few drops of 0.1 M NaOH and 0.1 M HCl solution. Secondly, 150 mg of OH/R-AuNCs beads (blackish colour) were added. Flasks were shaken in electric oven at constant oscillation amplitude for 12 h, and
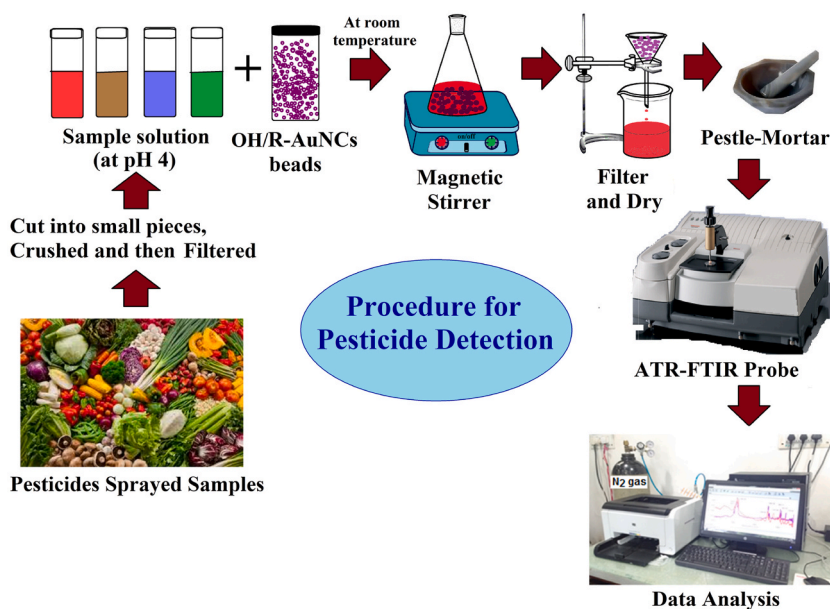
**Fig. 2.** Schematic representation of procedure for pesticide detection using OH/R-AuNCs as a substrate for SE/ATR-FTIR spectroscopy.
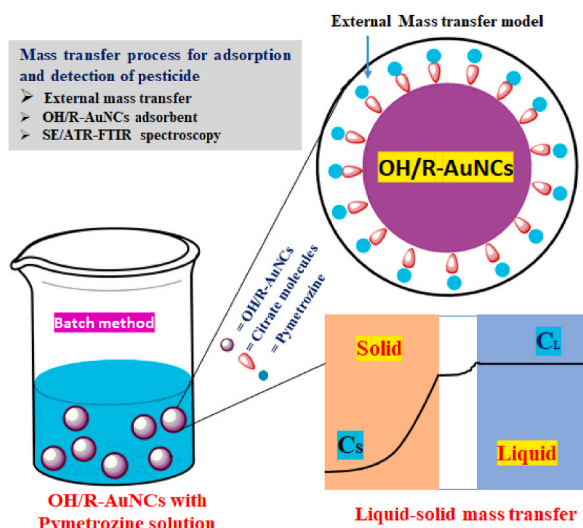


**Fig. 3.** Mass transfer process for adsorption and detection of pesticide.

then remained for 12 h to reach a complete adsorption during the external mass transfer process. The liquid to solid mass transfer process is shown in Fig. 3. Subsequently, a mixture of the sample's solution was filtered by using a 0.45 μm Whatman filter and extracted beads (dark-blackish colour) were dried at room temperature. Hereupon, approximately 15 mg of the dried pesticide adsorbed beads were finely ground using pestle-mortar with turn by turn and the powdered samples were directly placed onto the ZnSe crystal of the ATR-FTIR probe for spectral analysis.

### 2.6. Sorption isotherms and analytical validation

Among the several existing isotherms, the sorption data were subjected to three regularly used isotherms models, namely Langmuir, Freundlich, and Temkin, to evaluate the maximum adsorption efficiency of adsorbent [4]. The equilibrium of the adsorption was then studied to understand the adsorption mechanism of the target molecules onto OH/R-AuNCs beads [21,29]. The % adsorption was calculated using the ratio of peak intensity of the amounts of analytes adsorbed onto OH/R-AuNCs adsorbents and peak intensity of initial concentration of adsorbate solution. All obtained infrared spectra were filtered using the single step baseline correction and
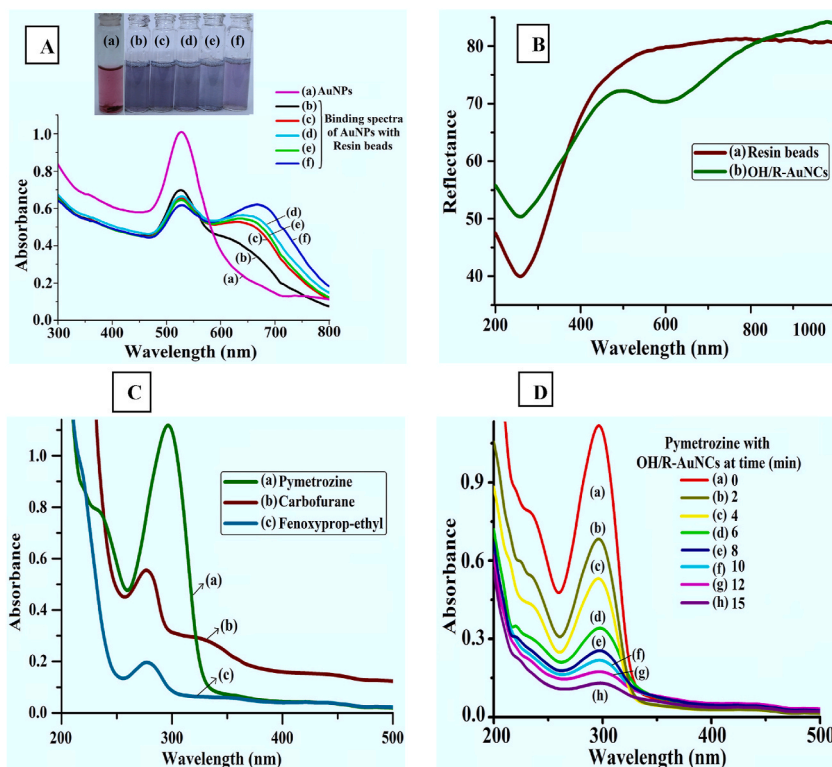
**Fig. 4.** (A) UV–Vis spectra of citrate-capped AuNPs (a), different amount of resin beads were added into the colloidal solution (b–f), (B) UV–Visible absorption spectrum of resin beads and OH/R-AuNCs with integrated sphere for powder sample (a–b), (C) UV–Vis spectra of pymetrozine, carbofurane and fenoxyprop-ethyl (a–c) and (D) Time dependent UV–Visible spectrum of OH/R-AuNCs in the presence of pymetrozine (a–h).

standardized by the software Omnic-9 TQ analyst (ThermoFisher, USA). All calibration standards were prepared by analyzing in the replicates of three. Peak areas under curve (AUC) corresponding to nitrogenous peaks ranging at 3019.94 cm$^{-1}$ (N-H stretching) for pesticide were utilized for quantification, and the calibration curve (CC) was obtained by averaging three replicate observations. Validation of the proposed methodology considered the different analytical parameters such as linearity, selectivity, limits of detection (LOD) and limits of quantification (LOQ), accuracy and precision and recovery %.

## 3. Results and discussion

### 3.1. Selection and characterization of prepared adsorbents

OH/R-AuNCs adsorbent were initially applied in electronics and biomedical applications owing to their extraordinary properties such as particle size and shape, uniform size distribution, crystal structure, elemental composition, purity, stabilization, reproducibility and higher mass production [22,30]. Some other properties such as large surface area to volume ratio, ease of chemical or physical modification, feasible regeneration, environmental soundness, the ability to remove environmental toxicants have been seen [23,31]. In comparison to our previous work, in which R-AuNCs adsorbent with a wide surface area can successfully remove dye molecules [21] from water sample. In ATR-FTIR spectroscopy, an evescent wave of reflectance electromagnetic radiation fell on the surface of nanocomposite materials, resulting in a high signal intensity for R-AuNCs. According to these physicochemical properties, a novel type of adsorbent was used for the sensing of pesticide from real sample matrices in this study.

Subsequently, the nanocomposite substrate was characterized by a UV–Visible spectrophotometer, SEM with EDX, and FTIR spectrophotometer. The optical properties of citrate-capped AuNPs and OH/R-AuNCs are investigated using UV–Vis spectrophotometer. The UV–Vis absorption spectrum shows a shoulder peak around 525 nm, which is attributed to the π- π* transition of aromatic sp$^2$ domains and n-π* transition of numbers of functional groups, respectively (Fig. 4(A)(a). Fig. 4(A)(b-f) shows UV–visible spectra of AuNPs after addition of different amounts of chlorinated resin beads due to the immobilization process. The localized surface plasmon resonance (LSPR) spectrum exhibits red-shifting at $\lambda_{max}$ 685 nm, resulting in nanoparticle aggregation caused by electrostatic interaction between citrate-capped AuNPs and resin matrix. During the mass transfer process, the red colour of the nanoparticle solution was turned into blackish colour resin beads when the AuNPs were completely immobilized on the resin, resulting in the absorption band of the NPs being not visible onscreen. These were also validated by acquiring a UV–Visible spectrum with a solid-state integrated sphere. The spectra obtained are shown in Fig. 4(B) (a-b). The UV–Visible absorption spectrum was also measured for the standard
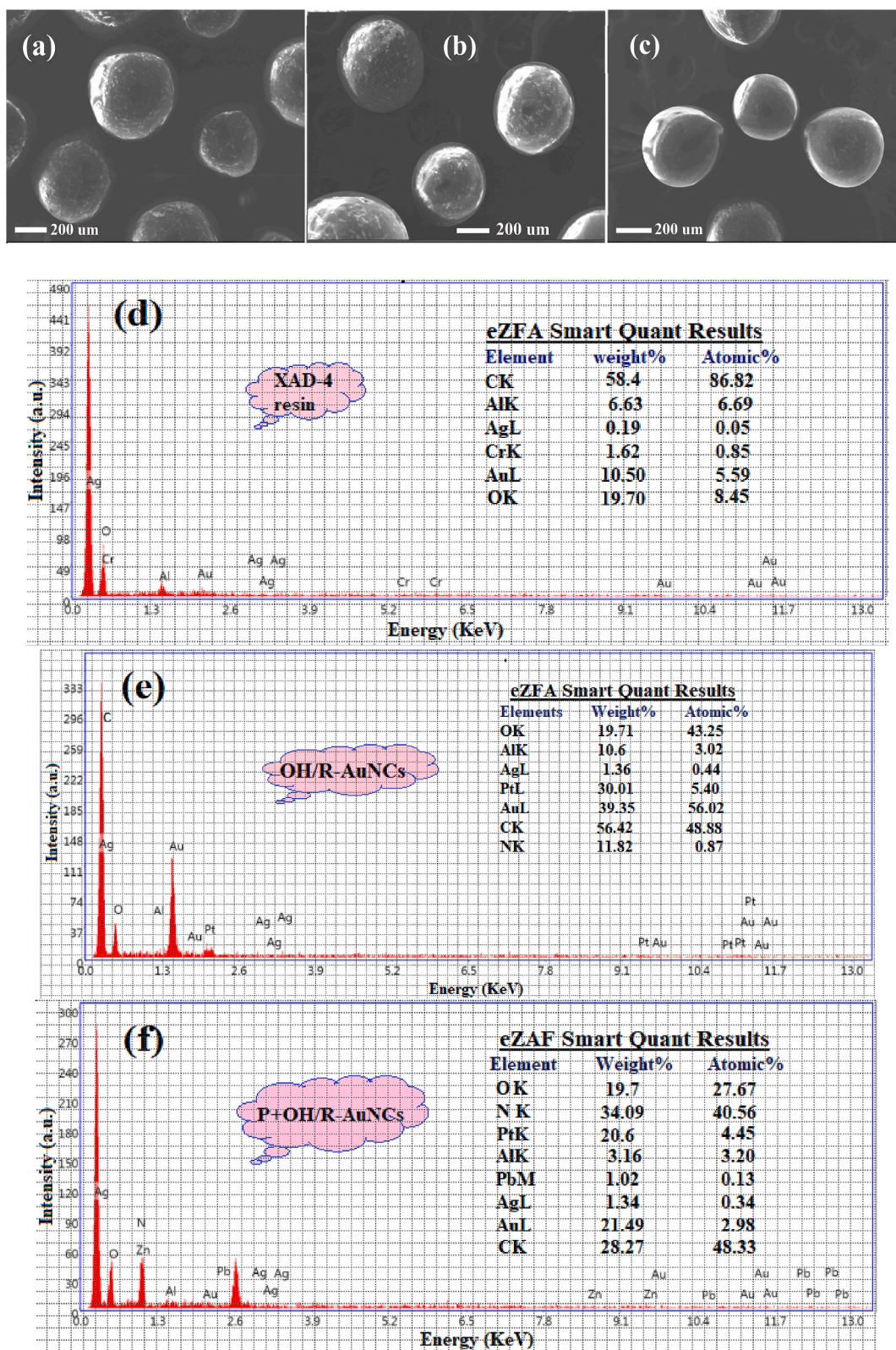
**Fig. 5.** SEM image of (a) amberlite XAD-4 resin, (b) OH/R-AuNCs, (c) pymetrozine with OH/R-AuNCs and SEM-EDX spectra of (d) amberlite XAD-4 resin, (e) OH/R-AuNCs and (f) pymetrozine with OH/R-AuNCs with observed eZAF smart quant results for elemental compositions.
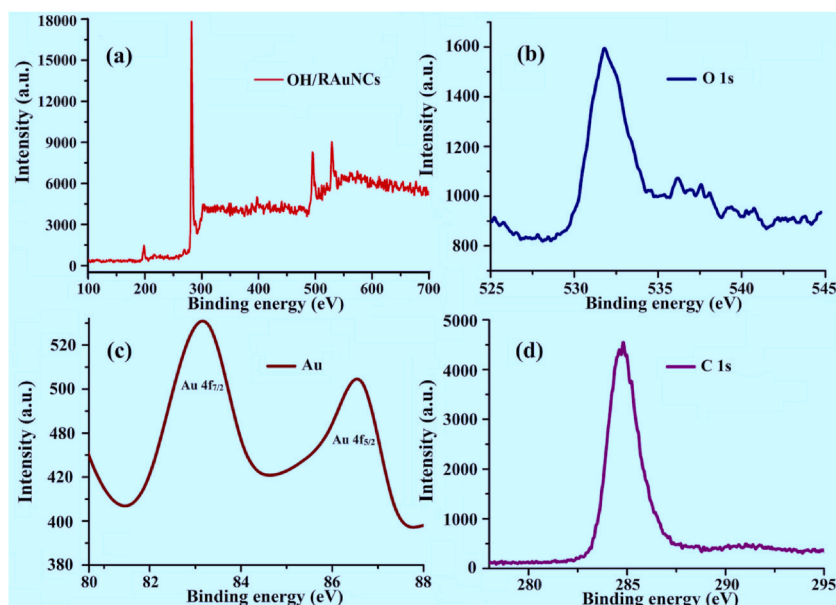
**Fig. 6.** XPS spectra of: (a) OH/R-AuNCs, (b) high resolution spectra of oxygen (O), (c) gold (Au) and (d) carbon (C) by survey scan.

concentrations of all pesticide (pymetrozine, carbofurane and fenoxyprop-ethyl) solutions (Fig. 4(C)(a-c)). The high absorption band at 290 nm was obtained for pymetrozine insecticide as compared to carbofurane and fenoxyprop-ethyl.

Next, time dependent UV–Visible spectra showing the adsorption of pymetrozine on OH/R-AuNCs as adsorbents (Fig. 4(D) (a-h)). The absorption spectrum of pymetrozine onto OH/R-AuNCs showing the absorption maximum at 290 nm. After 0–15 min, the plasmon excitation absorption at 290 nm continuously decreases in intensity and another broad absorption feature emerged at longer wavelength. At this stage the solution turns dark blackish in color. This can be attributed to the beginning of adsorption of pymetrozine on OH/R-AuNCs surface and their subsequent aggregation through electrostatic force of attraction along with mass transfer phenomenon. With further passage of time, the plasmon absorption at 290 nm decreases in intensity and that at longer wavelength, gains in intensity it accompanied by further red shift. This is due to the time-dependent adsorption of pymetrozine on the nanoparticles' surfaces. After 15 min, the completely analytes particles begin to transfer through a physicochemical adsorption and a mass transfer process (Fig. 3).

The attribute morphology, size and elemental composition of Amberlite XAD-4 resin and synthesized OH/R-AuNCs were carried out with SEM-EDX analysis. Fig. 5 illustrates the SEM images of Amberlite XAD-4 resin matrix (a), OH/R-AuNCs (b) and pymetrozine adsorbed onto OH/R-AuNCs surface (c). From the obtained images, it may be supposed that after the interaction, i.e., physicochemical adsorption of pymetrozine pesticide onto the surface of R-AuNCs have quite surrounded by a silky layer either a rough and plane surface of XAD-4 resin as compared to the modified OH/R-AuNCs adsorbents. The size of pores in the resin and resin immobilized gold nanocomposite materials were found to be less than 5 nm (micropores, 50 A) of the pore radius. Similarly, greater than 2 nm diameter pore size of AuNPs was found. Fig. 5(a–c) display the particle size and surface morphology of OH/R-AuNCs in absence and presence of analytes, it is located that with the addition of pymetrozine, the surface regions and pore volumes of the debris decrease, but the pore sizes of the debris were expanded, this means that that the pore systems had been changed with the addition of target analyte. In addition, there was no extra reactive site in OH/R-AuNCs and a few molecules were embedded inside the resin beads, whereas most of them could be seen on the surface of the OH/R-AuNCs. It turned to be determined that OH/R-AuNCs exhibited mass transfer into the adsorbents with a median lateral length of $5.60 \pm 2.42$ nm. To further evaluate the elemental composition of individual points or to map out the lateral distribution of elements from the imaged area of XAD-4 resin beads, OH/R-AuNCs with and without adsorption of pymetrozine, energy dispersive spectroscopy (EDX) and elemental mapping of elements were also investigated [21,22]. EDX analysis was used to confirm the presence of carbon (58.4 %), oxygen (19.7 %), aluminium (6.63), chromium (1.62 %), gold (10.5 %) and silver (0.91 %) in the XAD-4 resin beads (Fig. 5(d)). Using the same technique, the presence of carbon (56.4 %), nitrogen (11.82 %), oxygen (19.7 %), gold (39.3 %), and silver (1.36 %), aluminium (10.6 %), platinum (30.01 %) was confirmed in the OH/R-AuNCs (Fig. 5(e)) [21] and these results were approximately similar with results obtained for XAD-4 resin beads. EDX analysis was confirming the presence of carbon (28.2 %), oxygen (19.7 %), nitrogen (34.0), platinum (20.6 %), gold (21.4 %), aluminium (3.16 %), lead (1.02 %) and silver (1.34 %) in the pesticide after adsorption onto OH/R-AuNCs during mass transfer process (Fig. 5(f)). (The elements abbreviation used in the tables are respected for O = oxygen, C = carbon, N = nitrogen, Al = aluminium, Zn = zinc, Ag = silver, Pt = platinum, Au = gold and Pb = lead) (Fig. 5(d–f)). The presence of Au in OH/R-AuNCs is found at 39.35 % according to the result of SEM with EDX analysis, which confirms the immobilization of AuNPs on the XAD-4 resin matrix.

Next, the XPS was used to acquire additional structural insight and to confirm the presence of a number of species on OH/R-AuNCs. The XPS spectrum shows peaks corresponding to OH/R-AuNCs and the high-resolution spectra of gold (Au), oxygen (O) and carbon (C) (Fig. 6(a)). Fig. 6(b) represents the high-resolution spectra acquired at a binding energy value of 533 eV due to O moiety. The peaks
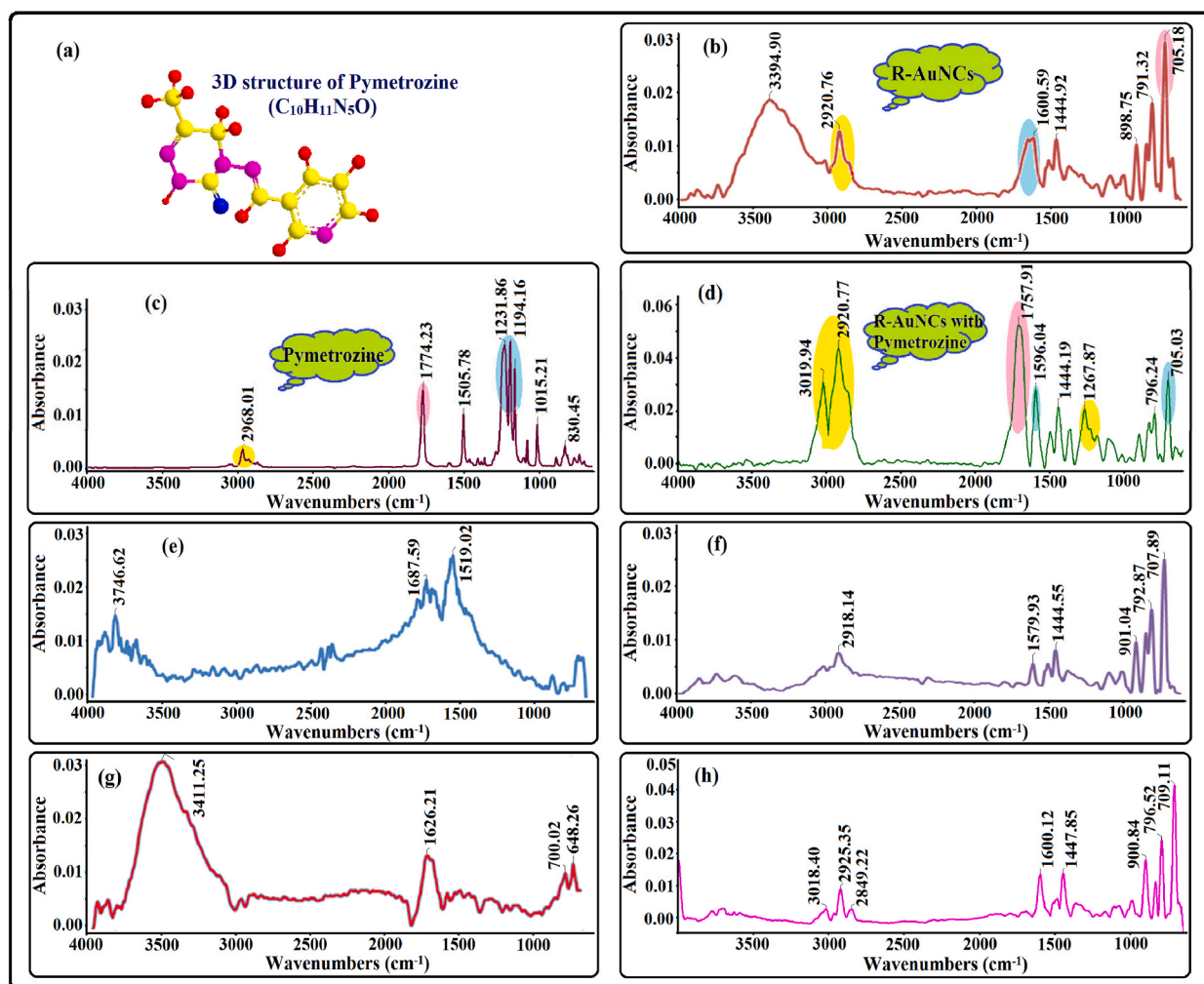
**Fig. 7.** 3D molecular structure of pymetrozine having molecular having formula $C_{10}H_{11}N_5O$ (a), ATR-FTIR spectral assignment of OH/R-AuNCs (b), pymetrozine (c), OH/R-AuNCs with pymetrozine (d), carbofuran (e), OH/R-AuNCs with carbofuran (f), fenoxaprop-ethyl (g) and OH/R-AuNCs with fenoxaprop-ethyl (h).

obtained at 83 eV and 87 eV correspond to the binding energies of Au4f$_{7/2}$ and Au4$_{5/2}$, respectively (Fig. 6(c)) [32]. Similarly, the intense peak at around 285 eV corresponds to the binding energy of C moiety present in resin nanocomposites (Fig. 6(d)). It means that upon binding of C, O and Au into the OH/R-AuNCs structure, it combines with the surface functional groups as well, confirming the presence of the binding of C, O and Au species on OH/R-AuNCs networks.

### 3.2. Spectral assignments of pesticides onto OH/R-AuNCs: a comparative study

FTIR is a simple analytical technique used for characterization and quality assurance of materials based on the functional groups, chemical bonding and molecular structures of chemical substances [33]. FTIR spectroscopy has gained wide acceptance in this field by virtue of its remarkable usefulness for both qualitative and quantitative analysis. The electromagnetic mechanism plays a key role in signal enhancement, while molecules in solution is also chemisorbed on the surface of nanocomposite materials, thus opening the possibility for chemical changes [33,34]. Despite the fact that there have been not many reports about its application in identifying pesticide residues, SE/ATR-FTIR in the middle wavelength range shows stronger potential for the quantification of pesticide residues on the surface of OH/R-AuNCs adsorbents. Recently, our research team has exploited SE/ATR-FTIR for the quantitative detection of glutathione, methylene blue dye and surfactant using functionalized AgNPs in biological and environmental samples based on the measurement of the characteristic absorption peak of analyte in the obtained IR spectra [20–22,33].

In this current work, a pilot research was performed in order to optimize the measurements of the SE/ATR-FTIR spectra with the ATR accessories and to evaluate the information content and comparisons of the spectra of different pesticides with and without using OH/R-AuNCs (Table S1). A change in path difference is accomplished by moving one of the two mirrors at a constant velocity over a

fixed distance. When the mirror has travelled the required distance, which is governed by the required spectral resolution, it is quickly returned to the start position to begin the next scan. As a result, we have got high signal with good resolution [33,34]. Therefore, the IR signal of the target was enhanced with changing the path difference. The present work, SE/ATR-FTIR time dependent method was employed for the complete adsorption of pesticide onto the surface of R-AuNCs materials. The initial experiment was performed to determine different spectral bands of pymetrozine, carbofuran, fenoxaprop-ethyl with and without OH/R-AuNCs. The standard solutions of individual pesticides and OH/R-AuNCs were analyzed by SE/ATR-FTIR to identify the characteristic infrared absorption peaks under the optimized conditions. The molecular structure of all organophosphorus pesticides consists of a two to five-membered N-heterocyclic ring containing many nitrogen atoms and double bonds separated by a single bond, thus constituting a $\pi-\pi$ conjugated system. Fig. 7 displays the characteristic FTIR absorption spectra of pymetrozine, carbofuran, fenoxaprop-ethyl with and without presence of OH/R-AuNCs when changing in mirror velocities. Well-resolved peaks in the spectra could be successfully interpreted. The FTIR spectrum of OH/R-AuNCs shows peaks at 1600.59 cm$^{-1}$ and 1444.92 cm$^{-1}$ that corresponds to the COO$^{-}$ stretching vibration due to the immobilization of citrate functionalized AuNPs (Fig. 7(b)). Two absorption peaks at around 3393.90 cm$^{-1}$ and 2920.76 cm$^{-1}$ were assigned to the O-H stretching vibrations and C-H symmetrical stretching, respectively, which are indicating the capping of tri-sodium citrate molecules onto OH/R-AuNCs surface contain Amberlite resin matrix. Fig. 7(c) shows the FTIR spectra of pymetrozine and spectral bands are ascribed to dissimilar functional groups. The FTIR spectra of pymetrozine shows strong peaks at 2968.01 cm$^{-1}$ (N-H stretching), 1774.23 cm$^{-1}$ (C=O stretching), 1505.78–1500 cm$^{-1}$ (N-H bending vibration), 1231.86 cm$^{-1}$ (amine C-N stretching), 1194.16 cm$^{-1}$ (C-C stretching), and 830.45 cm$^{-1}$ (C=C bending vibration). Fig. 7 (d) shows the IR absorption spectra of OH/R-AuNCs after the adsorption of pymetrozine. For the nitrogen hybrid ring and amine group containing pymetrozine standard solution, a strong peak was obtained at 2968.01 cm$^{-1}$, corresponding to the N-H stretching. The band shifted from 2968.01 to 3019.94 cm$^{-1}$ (N-H stretching) when pymetrozine was bound onto the surface of OH/R-AuNCs through H-bonding and $\pi$-$\pi$ stacking interaction between them. It results in enhancement in the peak intensity of OH/R-AuNCs at ~2920.77 cm$^{-1}$ for C-H stretching, indicating that the interaction via adsorption of pymetrozine with OH/R-AuNCs has really occurred. The FTIR spectrum of carbofuran was recorded before and after assimilation with OH/R-AuNCs beads, a prominent peak was observed between 1687.59 cm$^{-1}$ to 1680 cm$^{-1}$, which was assigned to the C=O stretching of the secondary amide compound. The other absorption bands for carbofuran added OH/R-AuNCs were obtained with respect to R-AuNCs spectra and no enhancement in the OH/R-AuNCs spectrum was observed at the reaction condition. The results are shown in Fig. 7(e and f). Similarly, Fig. 7(g and h) shows the FTIR absorption spectra of fenoxaprop-ethyl with and without the addition of OH/R-AuNCs. Characteristic peaks observed at 3000 and 2800 cm$^{-1}$ correspond to N-H and C-H bond stretching, 1600.12 cm$^{-1}$ for C=O stretching, 1447.85 cm$^{-1}$ for C-H bending (methyl group), 796.52 to 709.11 cm$^{-1}$ for C=C bending vibration, respectively.

Based on these findings, we observed that the FTIR spectrum of OH/R-AuNCs with pymetrozine exhibits considerable signal amplification when compared to other pesticides under optimum reaction conditions such as 150 mg of NMs, 6.0 min reaction time at pH 4.0 during the mass transfer process. The absorption bands for all pesticides before and after adsorption onto OH/R-AuNCs surface is good agreement and no any results reported in the literatures [6,9]. Consequently, it could be regarded as the characteristic absorption bands for pymetrozine pesticides, thereby providing the basis for detecting organonitrogen pesticide residues.

### 3.3. Mechanism of signal enhancement of pesticide onto the OH/R-AuNCs: a physicochemical study

The mechanism for detecting pesticide onto the resin-nano matrix is demonstrated by performing dissimilar sets of experiments using OH/R-AuNCs as a substrate for time dependent SE/ATR-FTIR spectroscopy based on a mass transfer model. SE/ATR-FTIR spectroscopy detection using a time-dependent method based on different strategies is generally adopted from reviewing many literatures [6,9,17,21]. Time-dependent SE/ATR-FTIR spectroscopy is supported on the adsorption phenomena from the analyte solution to substrate employed, i.e., OH/R-AuNCs for spectral analysis. The process is aimed to use a new, simple and time resolved ATR-FTIR substrate on which the EMR fall and the spectra were collected. For this, 150 mg of prepared composite materials were added in a known quantity of individual pesticides such as pymetrozine, carbofuran and fenoxaprop-ethyl solution followed by FTIR analysis with ATR accessories under the optimized conditions. The models depict chemical (chemisorption) and physical (physicoadsorption) adsorption phenomena, as well as their application to the detection of pymetrozine pesticide at very low levels in vegetable samples. The importance of these phenomena is used to adsorb major quantities of analytes onto the surface of OH/R-AuNCs beads during the external mass transfer process and analyzed using SE/ATR-FTIR. The FTIR spectrum of target analyte adsorbed onto the surface of OH/R-AuNCs adsorbents is shown in Fig. 7(c and d) and Table S1. The physicochemical system is helps to enhance interaction between the analyte and nano-composite materials, resulting in increased signal intensity. The presence of AuNPs onto the resin matrix was identified by comparing its spectra with free resin beads and citrate capped AuNPs (Fig. S2). As shown in Figs. S2(a–c), the IR spectra of pure resin beads showed the anti-symmetric stretching vibrations at 2921.62 cm$^{-1}$ for C-H stretching and at 1637.84 cm$^{-1}$ for C=C stretching vibration. The characteristic spectral bands for AuNPs were obtained between 3200 and 3600 cm$^{-1}$ due to the broad O-H stretching vibration, at 1600.59 cm$^{-1}$ and 1444.92 cm$^{-1}$ attributed to C=O and C-H stretching of sodium citrate. All the characteristic spectral bands observed in OH/R-AuNCs confirm that each of the materials is bound together to form nanocomposites. Fig. 7(c and d) shows the SE/ATR-FTIR absorption spectrum of pymetrozine without and with the addition of OH/R-AuNCs material. Captivatingly, a band-shift from 2968.01 cm$^{-1}$ to 3019.94 cm$^{-1}$ (N-H stretching), assigned to the amine salt of pymetrozine was found after adsorption on the surface of OH/R-AuNCs because during the physicochemical adsorption process, the electronic–vibrational state of the analytes changes due to the contact of the resin immobilized metal nanoparticles surface. This is also assigned as a characteristic for adsorption of pymetrozine on OH/R-AuNCs, which act as hot-spot density when the reflected radiation interacts with pymetrozine adsorbed on the surface of OH/R-AuNCs beads [35]. The enhancement of the signal intensity is due to the adsorption of analytes onto the surface of
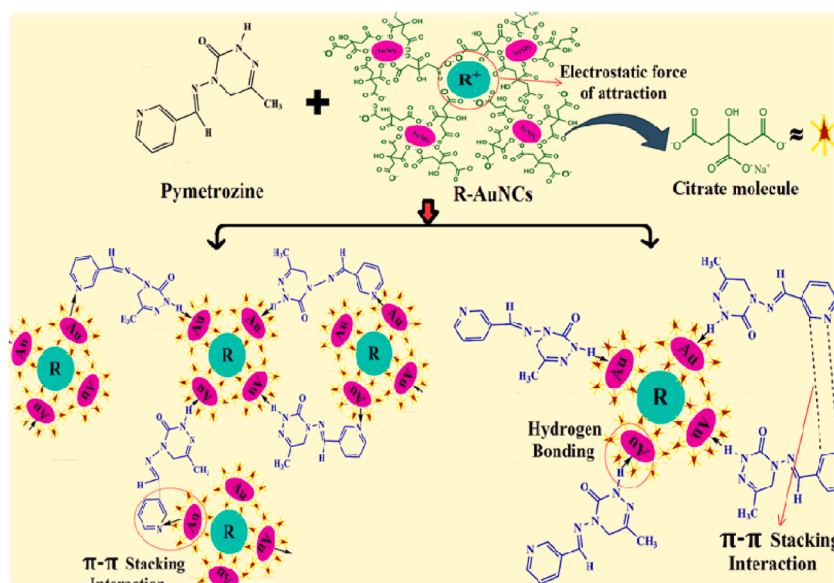
**Fig. 8.** Schematic representation of reaction pathway for pymetrozine determination using OH/R-AuNCs.

the substrate during mass transfer process, which increases the pre-concentration of the analyte on the surface of prepared OH/R-AuNCs materials. The main reason behind this was the presence of a maximum number of interaction sites such as four nitrogen hybrid rings and a secondary amine in pymetrozine pesticide. The adsorption of pymetrozine is also confirmed by the SEM, SEM-EDX and XPS data (Figs. 5 and 6). The determination via adsorption of pymetrozine onto the nanocomposites was also studied using UV–Visible spectroscopy, as shown in Fig. 4(A-D). The working solution of pymetrozine has a maximum absorbance in the 290 nm region. The UV–Visible absorbance of pymetrozine solution decreased as the reaction time was increased when 150 mg of OH/R-AuNCs were added to 5 mL of 10 µgmL$^{-1}$ pymetrozine solutions (Fig. 4(D)). In comparison to OH/R-AuNCs, the experiment using the same amount of pure resin beads of Amberlite XAD-4 resulted in a slighter drop in the absorbance of pymetrozine over time.

Based on this characteristic behaviour, we have illustrated the mechanism in the following conceptual theories for the detection of pesticide (Fig. 8). This process started from here, the association with the coordination of both oxygen atoms to gold surfaces due to the intramolecular interaction with the hydroxyl group of the adsorbed citrate ions. AuNPs were immobilized onto the resin beads through electrostatic force of attraction and ion exchange process along with chlorination. The prepared OH/R-AuNCs having a negative charged surface with the O atom react easily with the pesticide, which showed the intermolecular force of attraction via layer by layer adsorption phenomena of resin nano-composites [21]. This indicates that the adsorption model also depends on the amount of analyte adsorbed on the surface of the OH/R-AuNCs due to the external mass transfer process. The adsorption isotherm explains the distribution of pymetrozine pesticide between the liquid and the solid phase when the processes involved mass transfer. The % adsorption was confirmed by calculating the peak intensity of the amount of pymetrozine pesticide adsorbed on the surface of OH/R-AuNCs materials (Equation-I and II).

$$\% \text{ A dsorption} = \frac{PI_0 - PI_e}{PI_0} x\,100 \tag{I}$$

$$Q_e = (PI_o - PI_e)x\,\frac{V}{W} \tag{II}$$

Where, $Q_e$ represents the equilibrium ability of pymetrozine on OH/R-AuNCs, $PI_0$ and $PI_e$ is the peak intensity of initial and equilibrium concentration of adsorbate solution (µg mL$^{-1}$), respectively. V is the volume of the pymetrozine pesticide solution and W is the weight of the adsorbent. In our previous studies, we have already described the properties of OH/R-AuNCs along with the high adsorption efficiency and high binding affinity toward the targeted analytes in FTIR [21]. Therefore, the OH/R-AuNCs caused the effective absorption of electromagnetic waves in the region 4000-400 cm$^{-1}$ when they were used as an adsorbing material for the detection of pymetrozine pesticide from vegetable samples and this process is termed as SE/ATR-FTIR spectroscopy.

Now next, Freundlich isotherm, Langmuir isotherm and Temkin isotherm are presented by the following relations (Table S2). Where, $K_F$ denotes the Freundlich constant, a system property that indicates the adsorption capacity (mg g$^{-1}$) and adsorption intensity or surface heterogeneity, respectively. $C_e$ is the equilibrium pymetrozine pesticide concentration in solution (µg mL$^{-1}$), $Q_e$ is the equilibrium pesticide concentration on the OH/R-AuNCs (mg g$^{-1}$), $Q_0$ is the maximum adsorption capacity of the analyte per unit weight of adsorbent (mg g$^{-1}$), b is a constant related to the affinity of the binding sites (µg mL$^{-1}$), and $b_T$ and $a_T$ are constants related to the heat of adsorption and the equilibrium binding constant corresponding to the maximum binding energy, respectively. For monolayer adsorption onto a surface with a finite number of identical sites, the Langmuir isotherm is valid. The Temkin isotherm

reveals that the pymetrozine pesticide adsorption at 298K is characterized by a uniform distribution of binding energies up to some maximum binding energy [29]. Freundlich values ($28.26 \pm 0.87$ mg g$^{-1}$) indicated high adsorption capacity of pymetrozine pesticide onto OH/R-AuNCs when compared to the Langmuir isotherm model ($9.78 \pm 1.22$ mg g$^{-1}$), in which adsorption is based on the heterogeneous surface of adsorbents and Freundlich isotherm is not restricted to the formation of the monolayer [29]. The adsorption capacity of pymetrozine pesticide on the nano-composite was calculated using the Temkin isotherm model; the value is found to be $23.22 \pm 3.21$ mg g$^{-1}$. In addition, the percentage (%) adsorption was calculated using the peak intensity of the amount of pymetrozine pesticide adsorbed on the surface of OH/R-AuNCs adsorbents with different factors. Table S2 shows the isotherm characteristic with estimated batch method along with the physicochemical method, common formula, linear formula, formula constant and values of the adsorption isotherm.

According to the previous literature, a strong interaction between functionalized OH/R-AuNCs with three-nitrogen hybrid rings and exo-cyclic amine groups containing pymetrozine could play an essential role in effective adsorption of analyte onto the surface of nanocomposite materials (NCMs) [6,36,37]. The primary amines group, through electron rich nitrogen atoms, are probably leaped onto the surface of metal nanoparticles through the coordinating interactions with the electron lack exterior of the nanomaterials [38]. In addition, the nitrogen atom of the aromatic ring also exhibits a strong binding affinity towards the NCMs. Therefore, in SE/ATR-FTIR spectroscopic assay, the pyridine resembling compounds are frequently used as an aggregation mediator. The pyridine resembling compounds are also used as a convey agent of AuNPs i.e., the standard form to complex form [39]. In the present work, pymetrozine having multiple binding sites, i.e., the four nitrogen hybrid rings and one exo-cyclic secondary amine group conducted the reaction mechanism (Fig. 8). When OH/R-AuNCs materials get in contact with pymetrozine molecule, the nitrogen hybrid ring of the analyte conducts the hydrogen bonding with free terminal COO$^-$ group present in OH/R-AuNCs materials. Similarly, the present exo-cyclic pyridine rings also interact with OH/R-AuNCs through π-π stacking and electrostatic interaction. Moreover, the pyridine rings present in pymetrozine is also capable of forming π-π stacking interactions between them (Fig. 8). As a result, the adsorption of pymetrozine may induce the surface area of OH/R-AuNCs substrate, which appears to enhance the signal intensity of OH/R-AuNCs in the mid-IR region at 4000-400 cm$^{-1}$. Furthermore, the characteristic property of OH/R-AuNCs having a high surface to volume ratio ensures its interaction and adsorbed pymetrozine onto its surface and causes enhancement in the signal intensity (3019.94 cm$^{-1}$, N-H stretching) of ATR-FTIR analysis. It can also be observed from Fig. 7(c and d) that the IR peak intensity of the nanocomposite characteristic band for C-H at ~2920.76 cm$^{-1}$ was enhanced to more than 3-fold, possibly due to the interaction between pymetrozine pesticide and OH/R-AuNCs. The possible interaction/adsorption mechanism for pymetrozine with OH/R-AuNCs is shown in Fig. 7(d). In order to confirm that the pymetrozine is indeed adsorbed on nanocomposites surfaces, a control experiment was performed by treating pure OH/R-AuNCs with another class of pesticides solution under the same experimental conditions. There was decrease in the signal intensity and absorption efficiency of pesticides, implying the inability of activated OH/R-AuNCs alone to mass transfer it (Fig. 7 (e–h)). Moreover, the main reason for this is that the late adsorption/interaction with the same physical conditions for other pesticides might be due to the presence of less nitrogen hybrid rings and amine groups, which cannot induce the surface area of OH/R-AuNCs. That is also probably attributed to the fewer binding sites for coordinating interaction and the weaker π-π stacking interaction between them and pyridine rings.

### 3.4. SE/ATR-FTIR spectral characteristics: a quantitative analysis

The object of this study was to find the measurement conditions that provide the best sensitivity and repeatability for pymetrozine determination. Next, in order to improvement of signal intensity and adsorption efficiency, the strong absorption band of pymetrozine were obtained at 3019.94 cm$^{-1}$ for N-H stretching was utilized for quantitative analysis of pymetrozine pesticide using OH/R-AuNCs in SE/ATR-FTIR spectroscopy. Peak area values were in general order of magnitude more sensitive than peak height ones [33]. However, the band at 3019.94 cm$^{-1}$ for N-H stretching was chosen because it does not overlap with any excipient bands, such as carbonyl and pyridine rings (Fig. 7(b–h)) and has a greater selectivity than the amine group band at 3019.94 cm$^{-1}$. As can be seen in Table S1, the selected band peak height values provided have a lower LOD than the area ones. So, this measurement mode was selected and corrected with a baseline established from 3019.94 cm$^{-1}$ to avoid the effect of the presence of water in the formulations, which can interfere with the pymetrozine determination. In addition, another well-resolved absorption bands were also used for the spectral interpretation as well as qualitative analysis in this present work. Above all, the IR peak intensity at 3019.94 cm$^{-1}$ for asymmetric stretching of N-H group is proportionally increased with increasing the concentration of pymetrozine (Figure S2 (a-b)). A linear relationship is exhibited between the absorption peak intensity and the pymetrozine content at 3019.94 cm$^{-1}$ peaks (Figure S2 (a-b)). As a result, the aforementioned absorption band was chosen as a quantifying peak for the selective detection of pymetrozine in SE/ATR-FTIR spectroscopy from various vegetable samples employing OH/R-AuNCs.

### 3.5. Factor affecting the signal intensity and their optimizations

Several parameters such as the effect of pH, time, stirring rate and amount of substrate were examined towards optimizing analytical conditions for the adsorption of pymetrozine pesticides onto the OH/R-AuNCs using the SE/ATR-FTIR spectroscopic method. The pymetrozine was selected as a representative compound for the optimization of the method. The sample solution of pymetrozine was monitored by allowing for the absorption peak obtained at 3019.94 cm$^{-1}$ for N-H stretching of the amine group in FTIR spectra.
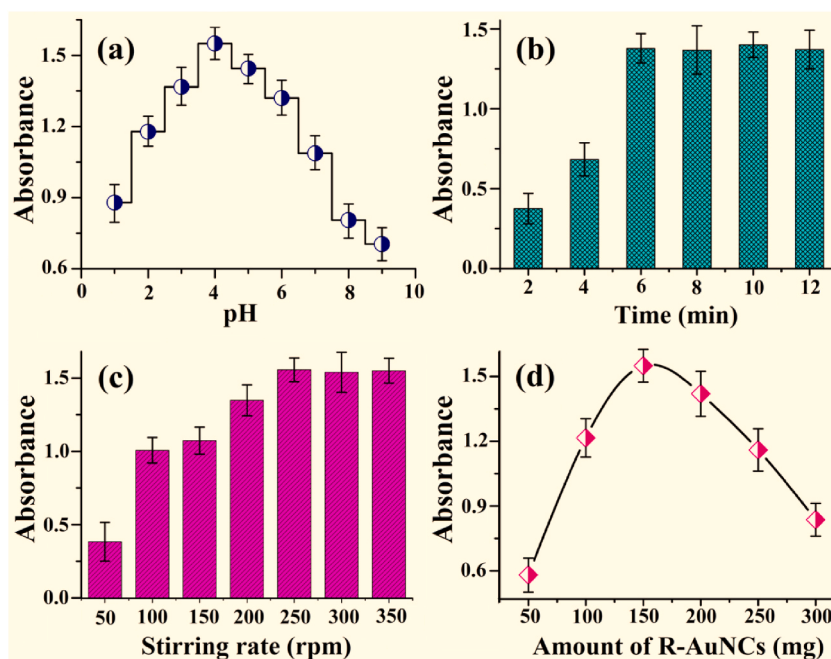
**Fig. 9.** Optimization of reaction conditions: (a) influence of pH, (b) effect of time, (c) effect of stirring rate and (d) effect of amount of OH/R-AuNCs beads for pymetrozine determination using SE/ATR-FTIR.

### 3.6. Influence of pH

Fig. 9(a) shows the adsorption for pymetrozine pesticides onto the OH/R-AuNCs at different pH values in the range 1.0–9.0. In this figure, the mass-based solid concentration, q (mg solute adsorbed per g resin beads) has been plotted against the initial liquid concentration, $C_i$ (in ppm). It will be noted from the data depicted in Fig. 9 (a) that the adsorption capacity of the analyte towards OH/R-AuNCs was the increased irrespective in the pH range from 1.0 to 4.0 (acidic medium) of the solution. However, in the case of basic medium, the solution pH decreased with the concentration of the electrolytes increased, leading to a greater degree of electrostatic repulsion with a resulting lowering of the adsorption capacity of the OH/R-AuNCs. Hence, the increasing presence of ions in solution at lower pH values would lead to a greater degree of electrostatic interaction and a consequent many folds increased in the adsorption capacity of the OH/R-AuNCs towards this pesticide.

### 3.7. Effect of surface assimilation time

The maximum transfer of pymetrozine from liquid phase to solid phase i.e., OH/R-AuNCs was scrutinized at different time intervals between 2.0 and 12 min. The results showed that higher signal intensity obtained at 3019.94 cm$^{-1}$ corresponding with N-H stretching for pymetrozine. As seen in Fig. 9(b), the adsorption efficiency reached its maximum value after 6.0 min for most of the pesticides evaluated. The signal intensity remained constant after 6.0 min, so the reaction time was fixed at 6.0 min for further studies.

### 3.8. Effect of stirring rate

The different stirring rate from 50 to 350 rpm was studied using a magnetic stirrer for the adsorption phenomena. The stirring rate was applied for adsorption of pymetrozine onto the OH/R-AuNCs during the phase transfer process. The effects of the change in stirring rate are shown in Fig. 9(c). The signal intensity of the pymetrozine with OH/R-AuNCs was increased with increasing stirring rate up to 250 rpm, above which no further improvement was observed. This constant result occurs due to the prolonging of the stirring rate, which originates the formation of bubbles in the resin bead, contributing to increased losses of the donor phase. Therefore, the 250-rpm stirring rate was fixed for the adsorption process.

### 3.9. Effect of amount of OH/R-AuNCs beads

The systematic studies were carried out to determine the optimal amount of OH/R-AuNCs in the pesticide solution. Fig. 9(d) shows the effect of varying the nanocomposites beads on the peak absorbance of pymetrozine at 3019.94 cm$^{-1}$ after 150 mg enrichment. The amounts of adsorbents, expressed as mg of OH/R-AuNCs beads in pymetrozine solution were varied from 50 to 300 mg. Fig. 9(d) indicates that a amounts of 150 mg adsorbents in pesticide solution is best compromise for optimum adsorption and signal response.
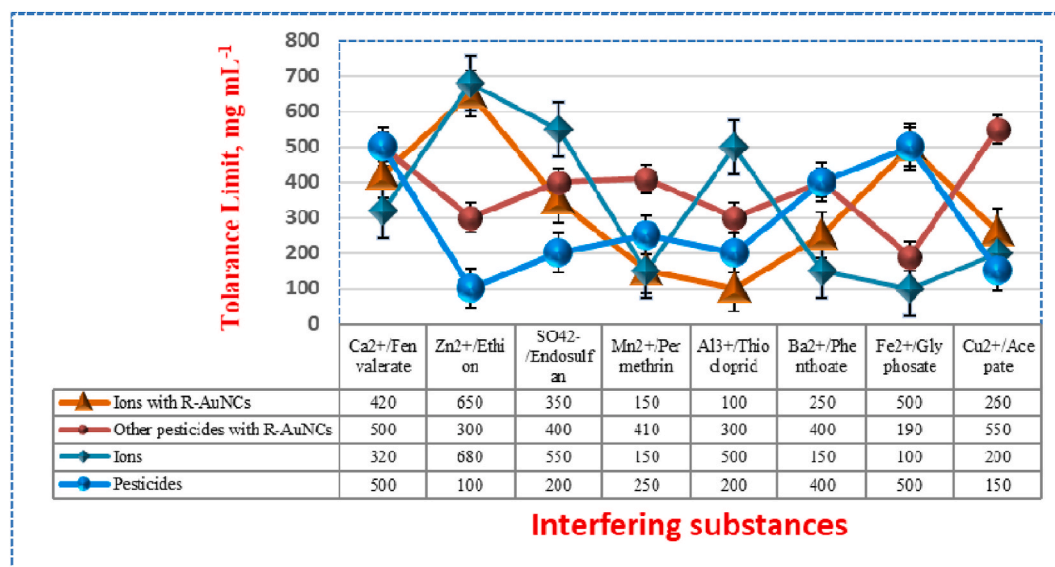
**Fig. 10.** Interference study for selective determination of pymetrozine in sample solution using OH/R-AuNCs with graphical representation to corresponding tolerance limits.

This study has shown that polar analyte such as pymetrozine pesticide show a different affinity for the nanocomposites than the non-polar compounds. Our studies also show that much smaller quantities of OH/R-AuNCs incorporated into the pesticide yield the optimum enrichment as well as signal enhancement. Therefore, the 150 mg of adsorbent was selected for the SE/ATR-FTIR spectroscopic method (Fig. 9(d)).

### 3.10. Effect of interfering ions and cross-contaminants: a selectivity study

Interference studies performed to selectively measure pymetrozine pesticide in sample solutions were investigated using OH/R-AuNCs as an adsorbent under optimized experimental conditions. Selectivity describes whether the methodology could discriminate interference of similar groups of compounds in the presence of the analytes, which is determined by relative absorbance value by SE/ATR-FTIR spectroscopic method [18,20]. None of the compounds tested for potential interference with the current method response caused any substantial interference. The key reason for these points, the phenomenon cannot be attributed to the fewer binding sites for coordinating interaction and the weaker π-π stacking interaction between them and the pyridine rings. The peak intensity of the analytes object did not change in the presence of the tested organic and inorganic chemical species of the proposed method. In addition, when we adsorb other pesticides on the resin surface, no adsorption process takes place whereas only pymetrozine pesticide does it during the physicochemical adsorption processes, which also results in a change in the colour (dark-blackish) of the resin beads. The experimental results of this investigation are given in Fig. 10. Therefore, it was found that this current method is free of interference from various substances and other pesticides commonly associated with the measurement of pymetrozine pesticide from vegetable samples.

### 3.11. Analytical validation for determination of pymetrozine using OH/R-AuNCs

The developed method was validated by determining the limit of detection (LOD), limit of quantification (LOQ), linearity range, correlation coefficient, relative standard deviation (RSD) inter-day and intra-day precision, and recovery % using OH/R-AuNCs in SE/ATR-FTIR spectroscopic method. Fifteen-time scans for ATR were accumulated per spectrum, with three reiterations per sample at time interval to get an average spectrum, and the obtained spectra were normalized against a KBr blank reference. Before data analysis, a Kubelka Munk theory is applied for smoothing the single step baseline. Employing this model, the optical properties of particular films under internal illumination can be predicted from the effective absorption and molecular extinction coefficients of the material. The calibration curve was showed a linear relationship between peak area and concentration over the range of 10–100 µg mL$^{-1}$ for pymetrozine pesticide (Fig. S3). The standard curve was created using ten calibration standards and proved to be reproducible throughout the calibration range. These ranges of concentrations were chosen in function of the sensitivity of the SE/ATR-FTIR spectroscopy towards target pesticide from the correlation coefficient ($R^2$) of the linear regression. The correlation coefficients ($R^2$) were also employed to ascertain the fit of all isotherms with the experimental data. The correlation coefficient ($R^2$) of the calibration curve was found to be $\geq 0.992$. LOD is the lowest concentration of analyte, which can be observed in an analyzed sample with a high degree of confidence. LOD is calculated by three times of standard deviation (SD) of three replicate measurements divided by the slope (b) value (i.e. LOD = 3SD/b). The value of LOD for the present work was calculated to be 2.65 µg mL$^{-1}$. LOQ is the smallest

**Table 2**
Recovery percentage (%) for determination of pymetrozine in tomato and potato samples collected from local market Raipur, using the proposed SE/ATR-FTIR spectroscopic method.

| S. No. | Samples[a] | Added pymetrozine (µg mL$^{-1}$) | Recovered concentration of pymetrozine[b] (µg mL$^{-1}$) | RSD (%) | Recovery (%) |
|---|---|---|---|---|---|
| 1. | Tomato 1 | – | $18.7 \pm 0.05$ | 0.3 | – |
| | | 20 | 39.6 | – | 104.5 |
| | | 50 | 67.8 | – | 98.2 |
| 2. | Tomato 2 | – | $21.9 \pm 0.15$ | 0.7 | – |
| | | 20 | 40.8 | – | 94.5 |
| | | 50 | 72.6 | – | 101.4 |
| 3. | Tomato 3 | – | $17.4 \pm 0.26$ | 1.5 | – |
| | | 20 | 36.9 | – | 97.5 |
| | | 50 | 69.0 | – | 103.2 |
| 4. | Potato 1 | – | $12.7 \pm 0.31$ | 2.4 | – |
| | | 20 | 32.5 | – | 99.0 |
| | | 50 | 63.0 | – | 100.6 |
| 5. | Potato 2 | – | $14.9 \pm 0.19$ | 1.3 | – |
| | | 20 | 35.8 | – | 104.5 |
| | | 50 | 66.1 | – | 102.4 |
| 6. | Potato 3 | – | $16.9 \pm 0.06$ | 0.4 | – |
| | | 20 | 36.2 | – | 96.5 |
| | | 50 | 67.8 | – | 101.8 |
| 7. | Brinjal 1 | – | $18.0 \pm 0.15$ | 0.8 | – |
| | | 20 | 37.8 | – | 99.0 |
| | | 50 | 67.6 | – | 99.2 |
| 8. | Brinjal 2 | – | $14.7 \pm 0.11$ | 0.7 | – |
| | | 20 | 36.7 | – | 110 |
| | | 50 | 65.5 | – | 101.6 |
| 9. | Brinjal 3 | – | $13.5 \pm 0.40$ | 2.9 | – |
| | | 20 | 33.8 | – | 101.5 |
| | | 50 | 63.2 | – | 99.4 |
| 10. | Green bell pepper 1 | – | $16.5 \pm 0.06$ | 0.4 | – |
| | | 20 | 37.0 | – | 102.5 |
| | | 50 | 66.3 | – | 99.6 |
| 11. | Green bell pepper 2 | – | $14.8 \pm 0.23$ | 1.6 | – |
| | | 20 | 34.4 | – | 98.0 |
| | | 50 | 64.7 | – | 99.8 |
| 12. | Green bell pepper 3 | – | $15.9 \pm 0.18$ | 1.1 | – |
| | | 20 | 35.6 | – | 98.5 |
| | | 50 | 66.3 | – | 100.8 |

[a] Samples collected from different regions of Raipur, Chhattisgarh, India.
[b] Average and standard deviation for n = 3 (SE/ATR-FTIR).

concentration of analyte, which can be distinguished and quantified at the known confidence level. It is analyzed by ten times of SD of three replicate measurements divided by the slope value (LOQ = 10SD/b) and for the existing method, the value of LOQ obtained was 8.75 µg mL$^{-1}$. Repeatability of the SEIRS instrument was checked using liquid standards prior to homogeneity studies. The repeatability of the method was estimated from the relative standard deviation of three independent measurements of the same aliquot positioned each time. Three replicates were analyzed at two different QC levels, i.e., 20 and 50 µg mL$^{-1}$. The relative standard deviation (RSD) for the analysis of QC samples in three replicates on three uninterrupted times was used to determine the assay's intra-day precision and inter-day precision. Accordingly, the intra-and inter-day precision was found in the range of 0.4 and 1.9 %, respectively for pymetrozine detection using OH/R-AuNCs in SE/ATR-FTIR spectroscopic method. Instrument consistently has the same results if it is used in the same situation on repeated experiment. The results obtained from the analytical evaluation are summarised in Table S3. In addition, the % adsorption was also calculated using the peak intensity of the amount of pymetrozine pesticide adsorbed on the surface of OH/R-AuNCs materials (according to above equation-I and II). The adsorption efficiency of the modified adsorbents was found to be 89.31 % in this present method. Moreover, the Freundlich isotherm, Langmuir isotherm and Temkin isotherm values was found to be $28.26 \pm 0.87$, $9.78 \pm 1.22$ and $23.22 \pm 3.21$ mg g$^{-1}$, respectively. The test values were found to be within the accepted variable limits on all occasions (validation parameters).

### 3.12. Application to vegetable samples

The advantages of method were successfully demonstrated for the detection of pymetrozine pesticide using OH/R-AuNCs from vegetable samples at very trace level based on chemical (chemisorption) and physical (physicoadsorption) adsorption phenomena. A total of 25 vegetable samples were tested, which were obtained from local market of Raipur city, Chhattisgarh, India. Out of these, 12 kinds of vegetable samples were found to be positive towards the presence of pymetrozine in significant concentrations. The results of positive samples having pymetrozine content have been shown in Table 2 and the FTIR spectra of real samples are shown in Fig. S4. Before treatment, the samples were stored at room temperature. Pymetrozine pesticide were the most frequently detected

**Table 3**

Comparison of present method with other reported methods along with technique, assisted probe, sample recognition, linearity range, LOD and recovery %.

| Analytical Technique | Assisted Probe | Recognition Sample | Linearity Range (µg mL$^{-1}$) | LOD (µg mL$^{-1}$) | Recovery (%) | Ref. |
|---|---|---|---|---|---|---|
| HPLC | – | Flue cured tobacco leaves | – | 0.005 | >90 | 5 |
| UV–Vis/Colorimetric | GNPs | – | 1–20 | <1 × 10-6 | – | 6 |
| Colorimetric | M-AuNPs | Water and food | $0.3 \times 10^{-5}$ -3.05 | 0.003 | – | 9 |
| DPP | – | Water and orange juice | 4.97, $10^{-7}$ | 1.48, $10^{-7}$ | 95 | 14 |
| SE/ATR-FTIR | OH/R-AuNCs | Vegetable | 10–100 | 2.65 | 94.5–110 | **Present Method** |

contaminants in all vegetable stuffs obtained from the sampling site as shown in Table 2. The sample preparation procedure is covered in the preceding section (2.3). Under optimal circumstances, the extracted samples containing pymetrozine insecticide with OH/R-AuNCs were subjected to SE/ATR-FTIR spectroscopy examination. A notable match of the SE/ATR-FTIR characteristic peaks at 3019.94 cm$^{-1}$ of pymetrozine and the vegetable samples peak confirmed the recognition of the target compound.

A quality control experiment was performed for all samples, consisting of the calibration standard in the matrix, blanks, and spiked samples for all the compounds. The concentrations of pymetrozine were determined in tomato, potato, brinjal and green bell pepper samples, and the same samples were also treated by spiking two different standards solutions of pesticides i.e., 20 and 50 µg mL$^{-1}$. Blank samples, considered to be those containing undetectable quantities of pymetrozine, were analyzed to evaluate the selectivity of the method. Thus, the blank samples did not show any signal at 3019.94 cm$^{-1}$ and nor kind of adsorption onto the R-AuNCs, indicating the absence of the analytes. But if we talk about the spiked process, pesticides were found in large quantities in the samples. Pymetrozine pesticide level in vegetables was found in the range of 12.7–21.9 µg mL$^{-1}$ and 32.5–72.6 µg mL$^{-1}$ without and with spiked process, respectively (Table 2). From this it is concluded that, highest concentration of pymetrozine (39.6–72.8 µg mL$^{-1}$) was detected in tomatoes, which indicates the recent use of the pymetrozine pesticide in the study area. The reliability of the existing method was determined by the analytical recovery % of added pymetrozine pesticide (Table 2). The mean analytical recovery % was obtained in the range of 94.5–110 % for pymetrozine pesticide. These results demonstrate that it is possible to use external calibration using vegetable samples-matched standards to accurately quantify the target compounds in the samples.

### 3.13. Comparison between the different strategies assayed

Detection of this pesticide from vegetable samples was monitored by SE/ATR-FTIR spectroscopy using OH/R-AuNCs materials and the adsorption of pesticides on nanocomposites was confirmed by mass transfer models. In order to show the advantages of the present OH/R-AuNCs system, the obtained results for the detection of pymetrozine from vegetable samples were compared with several reported adsorbents in the viewpoint of analytical technique, assisted probe, recognition sample, linearity range (µg mL$^{-1}$), LOD (µg mL$^{-1}$) and recovery (%) (Table 3) [5,6,9,14]. In this work, from the results, many-fold enhancements in the SE/ATR-FTIR spectroscopic signal can be achieved as well as five-times higher adsorption efficiency can be acquired using OH/R-AuNCs adsorbent as compared to those of GNPs and M-AuNPs [6,9]. The results were also compared with HPLC [5], UV–Vis/colorimetry [6], colorimetric [9] and DPP [14] techniques were found to be time-consuming, requirements high amounts of chemicals, expensive sample analysis and needs trained personnel. Using the current technique demonstrated that it is easy and cost-efficient for the detection of pymetrozine in vegetable samples based on a mass transfer model using novel substrate like OH/R-AuNCs. According to the SE/ATR-FTIR analysis of pymetrozine, we can more intuitively understand basic information regarding pesticide residues on tomato, potato, brinjal and green bell pepper samples surface.

## 4. Conclusions

In the present work, we productively and successfully synthesized the OH/R-AuNCs for the detection of pymetrozine in vegetable samples using SE/ATR-FTIR spectroscopy based on mass transfer phenomenon. The properties of OH/R-AuNCs like higher stability, reactivity, large surface area to volume ratio, feasible regeneration, and ability to remove organic and inorganic pollutants have made it used as a deliverable. The adsorption process is described using mass transfer models such as Freundlich, Langmuir and Temkin adsorption isotherms, which are best fitting the experimental data. The pesticide molecule binds to the OH/R-AuNCs through only one grouping and the adsorption becomes progressively easier as the absorbed quantity increases. The shape of these isotherms indicates that the pymetrozine is adsorbed as a monolayer and that there is no strong competition between the pesticide molecules and water to occupy the adsorption surface sites. The adsorption efficiency significantly influences the SE/ATR-FTIR response of the pymetrozine of above 89.31 %.

The construction of OH/R-AuNCs materials and adsorption phenomena for pesticide solution was confirmed by the results obtained from characteristic spectra of UV–Visible, SEM, EDX and XPS. In addition, many folds enhancement of the signal intensity of pymetrozine with OH/R-AuNCs was obtained compared to other pesticides with OH/R-AuNCs (i.e., carbofuran, fenoxaprop-ethyl) in SE/ATR-FTIR spectroscopic analysis. A good recovery range, i.e., 94.5–110 % was found for the present method. The advantages of the present method are being simple, easy to handle, rapid, cost effective, eco-friendly and non-requirement of sophisticated instrumentations and toxic chemicals. We thought it is worthwhile to explore the use of this technology for drinking water purification,

especially in rural areas of India where pesticide contamination is an important issue. These major outcomes have the potential to improve the methodology and technology used to detect pesticide residues for enhanced food safety.

## CRediT authorship contribution statement

**Anushree Saha:** Writing – original draft, Visualization, Validation, Methodology, Investigation, Formal analysis, Conceptualization. **Ramsingh Kurrey:** Writing – review & editing, Data curation. **Manas Kanti Deb:** Supervision, Software, Resources.

## Declaration of competing interest

The authors declare that they have no known competing financial interests or personal relationships that could have appeared to influence the work reported in this paper.

## Acknowledgement

## Appendix A. Supplementary data

Supplementary data to this article can be found online at https://doi.org/10.1016/j.heliyon.2024.e37856.

## References

[1] M.H. Dehghani, S. Ahmadi, S. Ghosh, M.S. Khan, A. Othmani, W.A. Khanday, K. Ansari, Sustainable remediation technologies for removal of pesticides as organic micro-pollutants from water environments: a review, Appl. Surf. Sci. 19 (2024) 100558.
[2] U. Jirata, T.G. Asere, Y. Buzayo, A. Gure, Levels of organochlorine pesticides in onion and tomato samples from selected towns of jimma zone, Ethiopia, Heliyon 10 (2024) e35033.
[3] M. Nasiri, H. Ahmadzadeh, A. Amiri, Sample preparation and extraction methods for pesticides in aquatic environments: a review, TrAC Trends Anal. Chem. 123 (2020) 115772.
[4] H. Sharma, A. Saha, A.K. Mishra, M.K. Rai, M.K. Deb, Diazotized reagent for spectrophotometric determination of glyphosate pesticide in environmental and agricultural samples, J. Indian Chem. Soc. 99 (7) (2022) 100483.
[5] V. Tripathy, S. Devi, G. Singh, R. Yadav, K. Sharma, R. Gupta, K. Tandekar, A. Verma, S. Kalra, Development and validation of tandem mass spectrometry-based method for the analysis of more than 400 pesticides in honey, J. Food Compos. Anal. 128 (2024) 106013.
[6] L.Y. Bai, Y.P. Zhang, J. Chen, X.M. Zhou, L.F. Hu, Rapid, sensitive and selective detection of pymetrozine using gold nanoparticles as colourimetric probes, Micro & Nano Lett. 5 (2010) 304–308.
[7] S. Mandal, R. Poi, D.K. Hazra, I. Ansary, S. Bhattacharyya, R. Karmakar, Review of extraction and detection techniques for the analysis of pesticide residues in fruits to evaluate food safety and make legislative decisions: challenges and anticipations, J. Chromatogr. B 1215 (2023) 123587.
[8] C. Bhatt, A. Saha, B.R. Khalkho, M.K. Rai, Spectroscopic determination of permethrin insecticide in environmental and agricultural samples using leuco crystal violet reagent, Environ. Sci. 3 (1) (2024) 14.
[9] J.Y. Kang, Y.J. Zhang, X. Li, C. Dong, H.Y. Liu, L.J. Miao, P.J. Low, Z.X. Gao, N.S. Hosmane, A.G. Wu, Rapid and sensitive colorimetric sensing of the insecticide pymetrozine using melamine-modified gold nanoparticles, Anal. Methods 10 (2018) 417–421.
[10] M.H. Khalifa, A.R. Khirallah, F.I. El-Shahawi, N.A. Mansour, H.K. Abou-Taleb, Field performance of selected insecticides on cotton aphid, Aphis gossypii and side effects on lady beetle, Coccinella septumpunctata, Arab J. Plant Prot. (2024) 208–214.
[11] S. Karmakar, R.K. Kole, S. Pan, G. Sarkar, P.C. Mondal, B. Horijan, Residue kinetics of insecticide pymetrozine in rice field soil, J. adv. biol. biotechnol. 27 (2) (2024) 226–239.
[12] W. Pan, Y. Lv, T. Pei, J. Li, S. Qin, F. Wang, L. Li, Method validation, dissipation and risk ranking of multi-pesticides in blueberry, J. Food Compos. Anal. 131 (2024) 106242.
[13] M. Gruba, E. Jóźwik, M. Chmiel, K. Tyśkiewicz, M. Konkol, A. Watros, K. Skalicka-Woźniak, G. Woźniakowski, Multi-residue method for pesticides determination in dried hops by liquid chromatography tandem mass spectrometry, Molecules 28 (13) (2023) 4989.
[14] H. Mercan, E. Yılmaz, R. Inam, Determination of insecticide pymetrozine by differential pulse polarography/application to lake water and orange juice, J. Hazard Mater. 141 (2007) 700–706.
[15] D.L. Jia, J. Gao, L. Wang, Y.D. Gao, B.X. Ye, Electrochemical behavior of the insecticide pymetrozine at an electrochemically pretreated glassy carbon electrode and its analytical application, Anal. Methods 7 (2015) 9100–9107.
[16] X. Yi, Z. Yuan, X. Yu, L. Zheng, C. Wang, Novel microneedle patch-based surface-enhanced Raman spectroscopy sensor for the detection of pesticide residues, ACS Appl. Mater. Interfaces 15 (4) (2023) 4873–4882.
[17] J. Wang, W. Ahmad, M.M. Hassan, M. Zareef, A. Viswadevarayalu, M. Arslan, H. Li, Q. Chen, Landing microextraction sediment phase onto surface enhanced Raman scattering to enhance sensitivity and selectivity for chromium speciation in food and environmental samples, Food Chem. 323 (2020) 126812.
[18] R. Kurrey, M.K. Deb, K. Shrivas, Methyl orange paired microextraction and diffuse reflectance-fourier transform infrared spectral monitoring for improved signal strength of total mixed cationic surfactants, J. Surfactants Deterg. 21 (2018) 197–208.
[19] S.M. Eid, K.M. Kelani, O.M. Badran, M.R. Rezk, M.R. Elghobashy, Surface enhanced infrared absorption spectroscopy (SEIRA) as a green analytical chemistry approach: coating of recycled aluminum TLC sheets with citrate capped silver nanoparticles for chemometric quantitative analysis of ternary mixtures as a green alternative to the traditional methods, Anal. Chim. Acta 1117 (2020) 60–73.
[20] B.R. Khalkho, R. Kurrey, M.K. Deb, I. Karbhal, S. Bahu, S. Sinha, Y.K. Sahu, V.K. Jain, A simple and convenient dry-state SEIRS method for glutathione detection based on citrate functionalized silver nanoparticles in human biological fluids, New J. Chem. 45 (2021) 1339–1354.
[21] A. Saha, R. Kurrey, M.K. Deb, S.K. Verma, Resin immobilized gold nanocomposites assisted surface enhanced infrared absorption (SEIRA) spectroscopy for improved surface assimilation of methylene blue from aqueous solution, Spectrochim. Acta Mol. Biomol. Spectrosc. 262 (2021) 120144.
[22] B.R. Khalkho, M.K. Deb, R. Kurrey, B. Sahu, A. Saha, T.K. Patle, K. Shrivas, Citrate functionalized gold nanoparticles assisted micro extraction of L-cysteine in milk and water samples using Fourier transform infrared spectroscopy, Spectrochim. Acta Mol. Biomol. Spectrosc. 267 (2022) 120523.

[23] A. Saha, Polymer nanocomposites: a review on recent advances in the field of green polymer nanocomposites, Curr. Nanosci. 20 (6) (2024) 706–716.
[24] R. Ningthoujam, Y.D. Singh, P.J. Babu, A. Tirkey, S. Pradhan, M. Sarma, Nanocatalyst in remediating environmental pollutants, Chemical Physics Impact 4 (2022) 100064.
[25] L. Kumar, V. Ragunathan, M. Chugh, N. Bharadvaja, Nanomaterials for remediation of contaminants: a review, Environ. Chem. Lett. 19 (4) (2021) 3139–3163.
[26] X. Zhao, L. Lv, B. Pan, W. Zhang, S. Zhang, Q. Zhang, Polymer-supported nanocomposites for environmental application: a review, Chem. Eng. J. 170 (2011) 381–394.
[27] A. Saha, M.K. Deb, M. Mahilang, R. Kurrey, S. Sinha, Polymeric resins as nano-catalysts: a brief review, J. Indian Chem. Soc. 97 (2020) 1–3.
[28] R. Kurrey, M. Mahilang, M.K. Deb, J. Nirmalkar, K. Shrivas, S. Pervez, M.K. Rai, J. Rai, A direct DRS-FTIR probe for rapid detection and quantification of fluoroquinolone antibiotics in poultry egg-yolk, Food Chem. 270 (2019) 459–466.
[29] J. Pal, M.K. Deb, Efficient adsorption of Congo red dye from aqueous solution using green synthesized coinage nanoparticles coated activated carbon beads, Appl. Nanosci. 4 (2014) 967–978.
[30] A. Saha, B.R. Khalkho, M.K. Deb, Au–Ag core–shell composite nanoparticles as a selective and sensitive plasmonic chemical probe for l-cysteine detection in Lens culinaris (lentils), RSC Adv. 11 (2021) 20380–20390.
[31] S.K. Verma, M.K. Deb, Nondestructive and rapid determination of nitrate in soil, dry deposits and aerosol samples using KBr-matrix with diffuse reflectance Fourier transform infrared spectroscopy (DRIFTS), Anal. Chim. Acta 582 (2007) 382–389.
[32] A. Saha, R. Kurrey, S.K. Verma, M.K. Deb, Cationic polystyrene resin bound silver nanocomposites assisted fourier transform infrared spectroscopy for enhanced catalytic reduction of 4-nitrophenol in aqueous medium, Chemistry 4 (4) (2022) 1757–1774.
[33] R. Kurrey, M.K. Deb, K. Shrivas, Surface enhanced infra-red spectroscopy with modified silver nanoparticles (AgNPs) for detection of quaternary ammonium cationic surfactants, New J. Chem. 43 (2019) 8109–8121.
[34] G. Rytwo, R. Zakai, B. Wicklein, The use of ATR-FTIR spectroscopy for quantification of adsorbed compounds, J. Spectrosc. 2015 (2015) 727595.
[35] A. Ravindran, N. Chandrasekaran, A. Mukherjee, Studies on differential behavior of silver nanoparticles towards thiol containing amino acids, Curr. Nanosci. 8 (2012) 141–149.
[36] F. Wei, R. Lam, S. Cheng, S. Lu, D. Ho, N. Li, Rapid detection of melamine in whole milk mediated by unmodified gold nanoparticles, Appl. Phys. Lett. 96 (2010) 133702–133705.
[37] G. Braun, I. Pavel, A.R. Morrill, D.S. Seferos, G.C. Bazan, N.O. Reich, M. Moskovits, Chemically patterned microspheres for controlled nanoparticle assembly in the construction of SERS hot spots, J. Am. Chem. Soc. 129 (2007) 7760–7761.
[38] D.I. Gittins, F. Caruso, Spontaneous phase transfer of nanoparticulate metals from organic to aqueous media, Angew. Chem., Int. Ed. 40 (2001) 3001–3004.
[39] G.B. Braun, S.J. Lee, T. Laurence, A.L. Et, Generalized approach to SERS-active nanomaterials via controlled nanoparticle linking, polymer encapsulation, and small-molecule infusion, J. Phys. Chem. 113 (2009) 13622–13629.